Selective adsorption, structure and dynamics of CO2 – CH4 mixture in Mg-MOF-74 and the influence of intercrystalline disorder

Dhiman, I.; Cole, David R.; Gautam, Siddharth

DOI
10.1016/j.chemphys.2025.112661

Publication date
2025

Document Version
Final published version

Published in
Chemical Physics

Chemical Physics 594 (2025) 112661

Contents lists available at ScienceDirect

Chemical Physics

journal homepage: www.elsevier.com/locate/chemphys

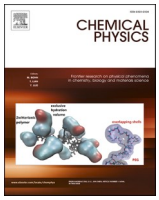

Selective adsorption, structure and dynamics of CO_2 – CH_4 mixture in Mg-MOF-74 and the influence of intercrystalline disorder

I. Dhiman [a,*], David R. Cole [b], Siddharth Gautam [b,*]

[a] Centre for Energy Research, Budapest, 1121 Hungary, Delft University of Technology, Mekelweg 15, Delft, 2629, JB, the Netherlands
[b] School of Earth Sciences, The Ohio State University, 275 Mendenhall Laboratory, 125 S Oval Drive, Columbus, OH 43210, USA

ARTICLE INFO

Keywords:
Mg-MOF-74
Selective adsorption
CO_2
CH_4
MD simulation
Diffusion
Intercrystalline space
Orientational disorder

ABSTRACT

Mg-MOF-74 is a highly efficient adsorbent for CO_2. We use molecular simulations to study the effects of disorder in Mg-MOF-74 on the selective adsorption, structure, and dynamics of a CO_2-CH_4 mixture. Positional disorder is introduced in the adsorbent by separating individual Mg-MOF-74 crystallites via inserting intercrystalline space between them. Rotating a crystallite with respect to others by different extents provides the orientational disorder (OD). Disorder is observed to enhance the adsorption selectivity of CO_2 over CH_4. The additional adsorption sites available by exposing crystallite surfaces may provide added selectivity for CO_2. Disorder is found to affect both the translational as well as rotational motion of CO_2 in Mg-MOF-74. This behavior follows a systematic pattern dictated by the interplay of the pore geometry of Mg-MOF-74 and Mg^{2+} – CO_2 interactions. Our results provide a guide on how to tailor Mg-MOF-74 adsorption behavior with desired properties by purposeful introduction of disorder.

1. Introduction

Gas mixture separation is one of the most ubiquitous processes relevant for environmental protection, energy production and for several industrial applications [1,2]. The removal and separation of several hazardous gases such as CO_2, N_2O, H_2S, CH_4, NH_3 etc., is of significant relevance for efficient energy production and environmental safety [2–14]. Of particular importance is the separation of CO_2 and CH_4 gas mixtures, present in natural and biogases [15,16]. Both CO_2 and CH_4 are the unsought components in the environment, therefore their removal from natural and biogas is crucial [15–21]. The presence of CO_2 in a humid environment leads to a formation of acidic solution which may in turn cause corrosion of pipes and plugging problems in industry [22]. Furthermore, separation of CO_2 from CH_4 also favors overall increase in calorific energy of CH_4, with more energetically dense product [23]. There is a considerable demand for natural gas, light hydrocarbons relevant for heat production, or fuel cells. Further, there may come a time when we need to separate CO_2 and CH_4 from Direct Air Capture as CH_4 levels also continue to rise from varied anthropogenic sources.

There are several separation methods reported in literature. D'Alessandro et al. reported a comprehensive study summarizing various technologies for CO_2 capture [24]. Among these the most common separation technique used in large scale industries is aqueous amine scrubbing. This method is inefficient in both energetic and economic terms and has potential harmful ramifications [25,26]. Therefore, development of alternative energy efficient separation methods is essential. In this context, adsorption-based techniques have become highly desirable, particularly in industrial facilities where energy usage and operating costs need to be kept to a minimum [1,27]. With technological growth in recent years, more efficient and environmentally benign methods of CO_2 adsorption using solid adsorbents have been developed. The most common potential solid adsorbents investigated for decades include silicalites [28–33], zeolites [34–40], and more recently, carbon-based materials [41–45] or metal-organic frameworks (MOFs) [46–59]. For zeolites and activated carbon regeneration, cost is a limiting factor. Commercially available polymeric membranes also have a drawback due to low selectivity and permeability, with low thermal and chemical stability [60].

A newer class of crystalline nanomaterials known as MOFs have become the focus of much interest in recent years [61–63]. MOFs comprise metal nodes connected via organic ligands [64]. MOFs are structurally very diverse and extremely tunable. Their structure can be easily modified by altering the building blocks. This leads to a highly diverse, customized variety of topology and pore structures.

* Corresponding author.
E-mail addresses: indu.dhiman@ek-cer.hu (I. Dhiman), gautam.25@osu.edu (S. Gautam).

https://doi.org/10.1016/j.chemphys.2025.112661
Received 25 September 2024; Received in revised form 28 December 2024; Accepted 12 February 2025
Available online 14 February 2025

Furthermore, MOFs have a large surface area and pore volumes, making them a great candidate for wide applications, including gas separation [65–74]. This also implies that using the combination of its organic linkers and metal ions MOF properties can be tuned for the relevant application.

Mg-MOF-74 exhibits high selectivity of adsorption for CO_2 containing gas mixtures, with wide combinations, such as $CO_2/H_2O/N_2$, CO_2/H_2O, CH_4/CO_2 and also for other gas mixtures like CH_4/N_2, CH_4/NH_3, CH_4/H_2S, etc. [75–77]. According to the DFT study reported by Park et al. the ratio of coordinated unsaturated metal sites (CUS) to open metal sites (OMS) in MOFs leads to high affinity and capacity of CO_2 owing to its strong interaction with OMS [78]. The strong electrical field arises from the electronic density of the Mg^{2+} ions. This leads to a formation of strong coordination bond between the CO_2 electrons and empty orbitals of Mg ions. Further, Mg-MOF-74 also exhibits significant potential for thermal and moisture stability [79 – 83]. This is primarily due to its robust metal-ligand coordination and crystalline framework. Studies have shown that while exposure to water can induce dissociation reactions at the metal centers, leading to structural degradation, these effects can be mitigated by modifying the framework or employing stabilizing techniques. For example, enhancing hydrothermal stability has allowed the material to maintain its CO_2 adsorption capacity even after multiple cycles of adsorption and desorption, highlighting its resilience under operational conditions. While single component membranes have been used for biogas separations, mixed matrix membranes comprising of particles dispersed in organic polymer matrix have been found to provide better performance [84]. In some cases, metal-organic framework can provide the dispersed phase. For example, incorporating MOF-5 in a MMM showed a marked increase in selectivity for CH_4 [85]. Incorporating a MOF into an MMM can lead to disorder and hence it is important to study the effects of disorder in a MOF adsorbent on the adsorption and selectivity of gas mixtures.

For decades, molecular simulations have been performed on ideal crystals and only fewer studies have addressed the influence of structural disorder/defects. According to the study reported by Thornton et al. on UiO-66 MOF system, the presence of defects at high pressure favors CO_2 adsorption/uptake, but at the expense of mechanical strength [86]. Sarkisov et al. explored the role of defects in IRMOF-1 for Ar adsorption [87]. No significant impact on the adsorption isotherms was observed for up to 20 % missing linkers. Additionally, a review by Basdogan et al. highlighted the need of simulation studies in constraining the role of defects [88]. Recently, Vellamarthodika and Gautam performed grand canonical Monte Carlo (GCMC) simulations to study the importance of intercrystalline spacing and orientational disorder (OD) in ZSM-22 adsorbate for SO_2 absorption [89]. An enhancement in adsorption capacity with intercrystalline spacing and OD was observed. In our previously reported molecular dynamics (MD) study, we explored the role of intercrystalline spacing combined with correlation between structure and dynamics of pure CO_2 confined in Mg-MOF-74 system [90]. With the introduction of intercrystalline spacing strong adsorption sites are observed around the pore periphery, in addition to the weakly adsorbing sites at the pore center of Mg-MOF-74. This behavior is correlated with the strong electrostatic interaction between CO_2 electrons and OMS, as reported by Park et al. [78]. Due to the presence of these electrostatic interactions between Mg^{2+} ions of Mg-MOF-74 and CO_2, in the gas mixture of CO_2 and CH_4, greater selectivity for CO_2 in the presence of an apolar molecule like CH_4 is expected. In the earlier study, we observed that presence of intercrystalline space adds new adsorption sites at the surfaces of crystallites, where electrostatic interactions are dominant [90]. The intercrystalline space added induces a hierarchical porosity that is beneficial for adsorption. In the current work, we explore the influence of intercrystalline spacing/gap (IG) and the systematic variation of induced orientational disorder (OD) in Mg-MOF-74 on the gas mixture of CO_2 and CH_4. Our objectives are to 1.) investigate if the disorder introduced in the system – both positional as well as orientational – can enhance the adsorption selectivity of Mg-MOF-74 for a CO_2 – CH_4 mixture; 2.) investigate the role of OD on the structural distribution and dynamical properties of the CO_2 and CH_4 molecules in the mixed gas system; and 3.) investigate how the presence of CO_2 affects the behavior of CH_4 molecules in Mg-MOF-74 system and vice versa. The introduction of disorder in Mg-MOF-74 is found to enhance the adsorption selectivity of CO_2 from a CO_2 – CH_4 mixture and affect the behavior of both the fluids. These results have important implications for the separation industry. To the best of our knowledge, such a systematic study exploring the role of OD combined with intercrystalline spacing has not been reported.

We provide all details about the simulations including building of models, force-fields and the simulation packages used in section 2. In section 3 we report the main results on adsorption, structure, and dynamics of CO_2-CH_4 mixture in Mg-MOF-74. Trends observed in these results are explained and discussed in the light of literature in section 4. Finally, we summarize the main findings in section 5.

2. Simulation Details

2.1. Models

To model Mg-MOF-74 structure, we used the coordinates optimized by Yazaydin et al. [91]. A .cif file of this structure is available on internet [92]. Mg-MOF-74 has a trigonal structure with cell parameters a = 2.6136 nm; b = 2.6136 nm; c = 0.6942 nm; $\alpha = \beta = 90^\circ$ and $\gamma = 120^\circ$. The unit cell vector c was aligned with the Cartesian direction Z while the a-b plane was coincident with the Cartesian X-Y plane. A unit cell was replicated initially $(3 \times 3) \times 2$ times in the Cartesian plane X-Y and direction Z, respectively. This resulted in a strip-like cell with small width along Z – direction. In what follows, this strip-like cell is referred to as a crystallite. Three of these crystallites were placed side by side along Z - direction to get a supercell. The resulting supercell consists of $3 \times 3 \times 6$ unit cells, as shown in Fig. 1. Disorder was introduced in this supercell by insertion of intercrystalline space separating the three crystallites and systematically rotating the middle crystallite with respect to the others about an axis of rotation passing through the center of the crystallite and along the Z – direction (crystallographic direction c). This means that the rotation axis is perpendicular to the a-b plane of the crystallites and hence the rotation does not change their a-b plane meaning they remain parallel. As a result, 8 different model supercells differing in the degree and type of disorder were obtained. The model with no intercrystalline spacing or rotation added represents an ideal crystal of Mg-MOF-74 and is denoted NG (no gap). All other models have an intercrystalline gap (IG) of 5 Å inserted between the crystallites and are therefore referred to as IG models. These 7 IG models differ from each other by the angle with which the middle crystallite is rotated and are referred to as IG_OD-n where n is the angle of rotation of the crystallite (= 0, 5, 10, 15, 20, 25, and 30). Examples of the progression from 0 to 30° are schematized in Fig. 1. Parameters of the simulation cells corresponding to different models are also included in Table 1. Note that the number of atoms in all models adsorbents remains the same. Introduction of the intercrystalline space gives rise to a hierarchical porosity in the IG models, which is beneficial for an enhanced adsorption [90]. We further note that the porosity in the crystallites and the added intercrystalline space have different geometries. While the pores in the crystallites are cylindrical with a width of about 1 nm and thus effectively one-dimensional, the inter-crystalline space can be considered as a two-dimensional slit-like pore (although of a narrower width of 0.5 nm), with an effectively wider distribution of adsorption sites. This change in dimensionality of the pores has important consequences for the behavior of adsorbed species [93]. It is important to note that the thickness of the crystallite layer can affect the trend of adsorption quantitatively, but not qualitatively. While it would be useful and interesting to study the effects of crystallite thickness on the adsorption amounts, we believe the overall trends observed here on the effects of introducing positional and orientational disorder will remain valid irrespective of the crystallite

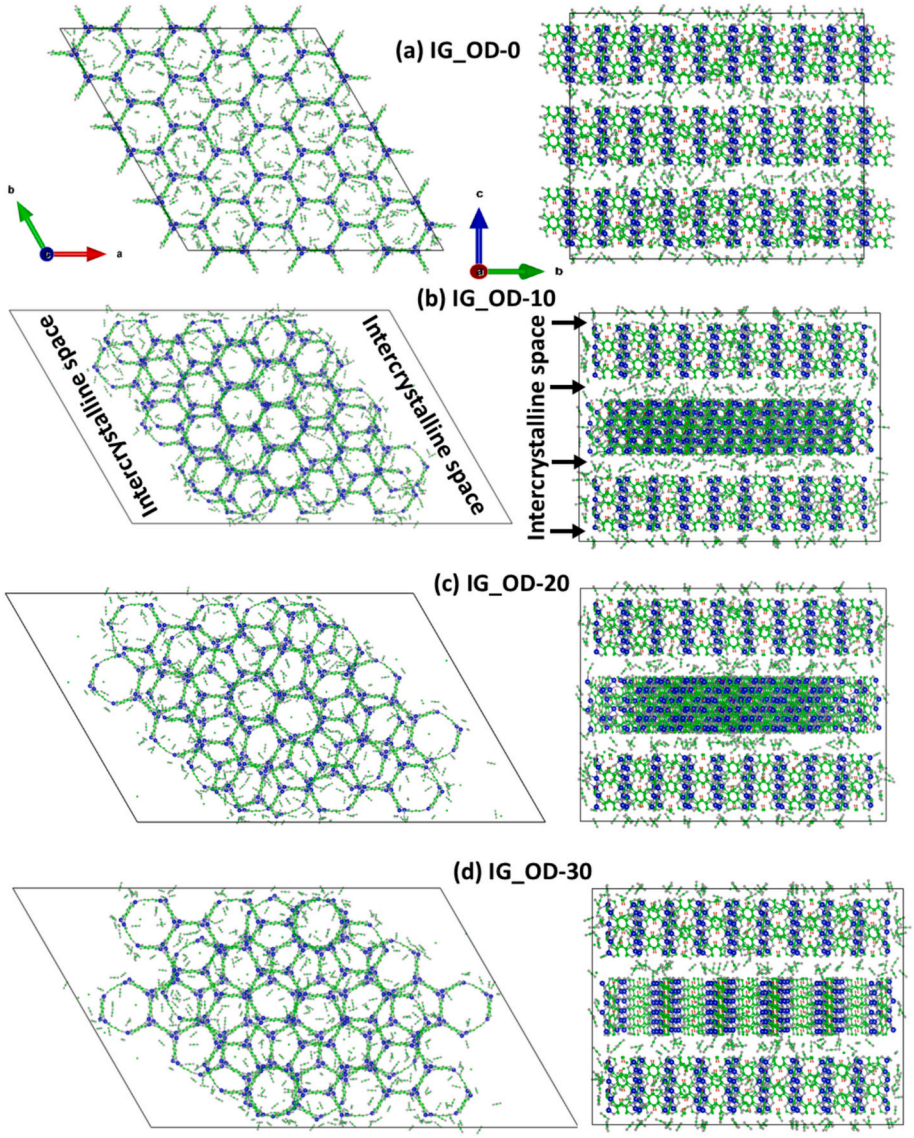

Fig. 1. (a) Simulation cell IG_OD_0 made up of 3 × 3 × 6 unit cells with intercrystalline spacing of 5 Å inserted in the *Z*-direction separating the three crystallites; without orientational disorder (OD), shown in the X-Y (left) and Y-Z (right) planes. The simulation cell boundary is marked with the black outline. (b) IG_OD-10 represents the simulation cell with intercrystalline gap and OD of 10° introduced by rotating the central crystallite. For ease of locating the intercrystalline space and avoid crowding, the intercrystalline space is marked in this panel alone, while the corresponding regions in other panels can be easily identified. (c) Simulation cell IG_OD-20, with 5 Å of intercrystalline spacing and OD of 20°. (d) Simulation cell IG_OD-30, with 5 Å of intercrystalline spacing and OD is induced by rotating the center crystallite by 30°. All the figures shown here are for loading of 510 CO_2 and 60 CH_4 molecules. Colour representation of atoms: Blue – Mg, Green – Carbon, Red – Hydrogen and Grey – Oxygen. (For interpretation of the references to colour in this figure legend, the reader is referred to the web version of this article.)

thickness. For computational affordability therefore, we chose to study crystallites made up of 2 unit cells in the crystallographic *c* direction. While three crystallites are needed to study the orientational disorder, the effect of inserting intercrystalline space without introducing orientational disorder can be studied using one crystallite. Therefore, in addition to all the models mentioned above, we also simulated a thicker crystallite with inter-crystalline space. This was made by inserting intercrystalline space only along the *Z*-direction (in X-Y plane) of width 0.5 nm to the NG model. This model represents a crystallite that is 3 times thicker than those in the IG models and is referred as LCG (large crystallite with inter-crystalline gaps). LCG differs from IG_OD0 only in the width of the crystallite and inter-crytalline space. Therefore investigation of this model is limited only to sorption and structural properties.

In the current study, we kept the MOF framework as well as the CO_2 molecules rigid. Methane is further modelled in the united atom formalism as a single structureless entity. This is in accordance to our previously reported study. We noted that the effects of framework flexibility on the diffusion of guest molecules in MOF reported in the literature are not clear and contradictory [65,76–78]. Additionally, simulating flexible system can be computationally demanding and expensive. Intramolecular interactions while being expensive are not expected to result in great differences at long time behavior, with the time scales that we are probing.

2.2. Grand canonical Monte Carlo Simulations for selective adsorption of an equimolar CH_4 - CO_2 mixture

Selective adsorption of an equimolar mixture of CH_4 and CO_2 in the eight models of Mg-MOF-74 described above was studied using grand canonical Monte Carlo (GCMC) simulations package DL_Monte [94]. These simulations employed a starting configuration with one of each adsorbate molecule (CO_2 and CH_4) placed in the simulation cell

Table 1
Properties of the different adsorbent structures studied and details of the corresponding simulation cell.

Adsorbent	Type of Disorder[1]	Rotation angle of the middle crystallite (degrees)	Simulation cell parameters[2] (nm)
NG	No disorder	0	a = 7.84; b = 7.84; c = 4.165
LCG	Only PD	0	a = 7.84; b = 7.84; c = 4.665
IG_OD-0	Only PD	0	a = 7.84; b = 7.84; c = 5.665
IG_OD-5	PD + OD	5	a = 13.329; b = 8.625; c = 5.665
IG_OD-10	PD + OD	10	a = 13.329; b = 8.625; c = 5.665
IG_OD-15	PD + OD	15	a = 13.329; b = 8.625; c = 5.665
IG_OD-20	PD + OD	20	a = 13.329; b = 8.625; c = 5.665
IG_OD-25	PD + OD	25	a = 13.329; b = 8.625; c = 5.665
IG_OD-30	PD + OD	30	a = 13.329; b = 8.625; c = 5.665

[1] PD is positional disorder; OD is orientational disorder.
[2] Only the lengths of the cell vectors are different for different structures, the angles remain the same, i.e. $\alpha = \beta = 90^\circ$ and $\gamma = 120^\circ$ for all adsorbents.

consisting of the Mg-MOF-74 models shown in Fig. 1. GCMC simulations were then carried out with a 0.5 atm (= 50.66 kPa) partial pressure of each component and temperature fixed at 298 K. As the simulation progressed, the adsorbate molecules could be inserted / deleted, translated or rotated with respective probabilities of 0.5, 0.25 and 0.25. The insertion (P_i) and deletion (P_d) of the adsorbate molecules followed the following selection rules.

$$P_i = min\{1(\beta VP)exp(-\beta\Delta U)/(N+1)\} \quad (1)$$

$$P_d = min\{1(N/\beta VP)exp(-\beta\Delta U)\} \quad (2)$$

where V is the simulation cell volume, P is the partial pressure of the gas, U represents the potential energy, N is the number of molecules and $\beta = k_BT$. In these simulations, the number of adsorbed molecules appropriate for the temperature and pressure conditions is obtained. These numbers exhibited fluctuations and systematic drifts for up to 5 million steps, after which they stabilized with fluctuations under reasonable limits, suggesting achievement of equilibrium. A total of 7 million Monte Carlo steps were carried out for each system. After discarding the first 5 million steps for equilibration, the average number of molecules of each species was calculated by averaging over configurations obtained in the remaining 2 million steps. The force field parameters are a combination of Dreiding and UFF [95]. CO_2 molecules are modelled using TraPPE force field and CH_4 molecules are modelled using united atom (UA) formalism [96,97]. To calculate the cross-terms the Lorentz–Berthelot mixing rules were used. The set of potential parameters are detailed in the supplementary materials file in Table S1. Agreement between experimental studies of CO_2 adsorption isotherms in Mg-MOF-74 and molecular simulations using this force-field has been shown previously by Yazayadin et al., Krishna, and Dietzel et al. [91,98,99].

2.3. Molecular dynamics simulations for quantifying structure, molecular orientation, translational and rotational dynamics

To investigate the structural and dynamical properties of the fluid mixture in Mg-MOF-74, classical molecular dynamics simulations were performed using the general-purpose software DL-POLY-v4.09 [100]. Mg-MOF-74, CO_2 and CH_4 are treated individually as non-vibrating rigid bodies. GCMC simulations yield an average number of 510 CO_2 and 60 CH_4 molecules adsorbed in the NG system at the conditions of temperature and pressure investigated. While IG models could adsorb a larger number of molecules, in MD simulations, the number of molecules in all models was kept the same for a fair comparison of dynamical properties. By doing this, we ensured that any change/contrast observed in the distribution of molecules with OD is solely a function of OD and not related to the variation in the number of molecules. Computational efficiency and the simulation stability was also considered.

For completeness we also performed MD simulations on NG and IG_OD-0 systems with pure CO_2 and CH_4 molecules. No significant change in the behavior of pure CO_2 and CH_4 molecules is observed when compared to the mixed CO_2 and CH_4 systems. This implies that CO_2 molecules may not have much influence on CH_4 molecules and vice – versa.

For these simulations, the dangling bonds at the crystallite surfaces have not been saturated. This is consistent with the previously reported studies by Dhiman et al. [90] and Gautam and Cole [101] that showed the CO_2 molecules are preferentially adsorbed at the periphery of pores of Mg-MOF-74 system. Therefore the dangling bonds are not expected to substantially affect the behavior of the adsorbate molecules.

NVT ensemble is used to perform simulations for 6 ns, trajectories saved after every 0.2 ps. The system is considered equilibrated when the energy and temperature fluctuations are below 5 %, which happened after 1 ns of simulation run. Therefore, the initial 1 ns is taken as equilibration time, while the remaining 5 ns as production run.

The obtained trajectories are unwrapped using the visual molecular dynamics (VMD) software tool. The long-range interactions are calculated using 3D Ewald sum. Periodic boundary conditions are applied along all the directions. TraPPE-force field convention with 14 Å cut off for all long-range Lennard-Jones interactions is used. A 1 fs integration step is used for all the simulations.

3. Results

3.1. Selective Adsorption of CO_2 in Mg-MOF-74 and the effect of disorder

Although the volume of the simulation cells for different structures studied here is different, the total number of atoms, and hence the adsorbent mass remains the same. As adsorption amounts are often compared normalized to the adsorbent mass, the variation of the absolute number of adsorbed molecules in adsorbents with the same mass would be the same except for a constant normalizing factor. We have therefore presented the un-normalized absolute adsorption in Figs. 2 (a) and (b). To highlight the effects of the inter-crystalline space, we have shown the number of each species adsorbed in the entire simulation cell, within the inter-crystalline space, and within the crystallites alone (discounting those that are adsorbed in the inter-crystalline space). Introduction of inter-crystalline space results in a redistribution of molecules between the crystallites and the additional inter-crystalline space. To obtain an estimate of the adsorption selectivity, in Fig. 2c we show the ratio of the number of adsorbed CO_2 to that of CH_4 molecules. Because the set partial pressures of the two adsorbates are equal, the mixture is equimolar and hence this ratio is identical to the adsorption selectivity. The number of adsorbed molecules obtained from the simulations had rather small uncertainties. However, the relative error involved in the estimate of the number of CH_4 molecules is significant because of very small amount of CH_4 adsorbed in the presence of a large amount of CO_2 and results in a large relative error in the estimates of selectivity. Nevertheless, it can be inferred beyond uncertainty that incorporating disorder in Mg-MOF-74 enhances the adsorption selectivity of CO_2 over CH_4. In the NG model, a selectivity of ~9 is obtained. This selectivity is enhanced significantly on the insertion of intercrystalline space (LCG and 0° rotation) and increases by almost a factor of two with respect to NG on the introduction of OD (5° rotation) when adsorption in the entire simulation cell is considered. If adsorption in the individual crystallites alone is considered, the selectivity remains the same within uncertainty for all systems. The enhancement in the selectivity is therefore a result of the enhancement in the inter-

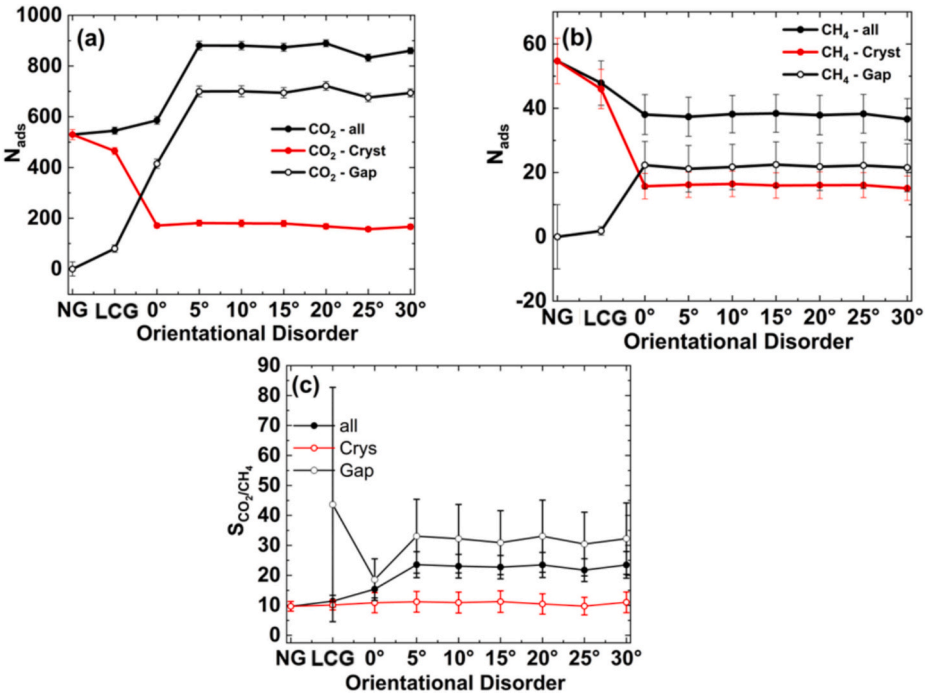

Fig. 2. (a) Number of CO_2 molecules adsorbed in the 8 models of Mg-MOF-74, within the crystallites (cryst), inter-crystalline space (gaps) and overall (all). The X - axis shows different models with the numbers (n) denoting the degrees of rotation of the middle crystallites in the IG_OD-n models. (b) Number of CH_4 molecules adsorbed in the 8 models of Mg-MOF-74, within the crystalline space, gaps and overall. (c) Adsorption selectivity of CO_2 over CH_4 in the 8 models of Mg-MOF-74, within the crystalline space, gaps and overall. The lines serve asa guide to the eye.

crystalline space alone where selectivity of more than 30 can be obtained for models with inter-crystalline space and a finite OD. Further, this enhancement is a result of higher CO_2 adsorption coupled with a lower CH_4 adsorption in the LCG and IG systems. However, increasing the extent of rotation of the middle crystallite further does not significantly alter the selectivity. In the following, we examine the structure and dynamics of CO_2 and CH_4 adsorbed in all these models of Mg-MOF-74.

3.2. Structure

Separate probability distribution maps of carbon atoms for CO_2 and CH_4 molecules in the mixture are calculated and plotted in XY-plane for the entire unit cell, as shown in Fig. 3(i) and Fig. 3(ii), respectively. The intensity plots in XZ and YZ-planes are shown in the supplemental section Figs. S1 and S2, respectively. The Z-intensity shown in Fig. 3(i) and (ii) is log (N + 1) where N represents the respective number of carbon atoms belonging to CO_2 (or CH_4) molecules that reside at a given location for some instant of time through the entire production run (10,000 time frames) in the XY-plane. The observed intensity is proportional to the probability distribution of finding a CO_2 (or CH_4) molecule at a given location and time.

For NG system (in Fig. 3(i)a), i. e., in the absence of intercrystalline spacing and OD, the CO_2 molecules prefer to occupy the periphery of Mg-MOF-74 pores. Six high intensity sites are observed around the pore periphery, where the CO_2 molecules are most likely to be localized. In addition, a few of the pore centers exhibit moderately high intensity regions. This behavior may be correlated with the presence of additional CO_2 molecules in the pores, wherein the adsorption of CO_2 molecules occurs once the peripheral sites are saturated. In contrast, CH_4 molecules are homogenously distributed around the pores of Mg-MOF-74 (in Fig. 3(ii)a), with a few of the pore centers exhibiting some occupancy. With the introduction of intercrystalline spacing and in the absence of OD for the LCG and IG_OD-0 systems, differing redistribution patterns of CO_2 (510) (in Fig. 3(i)b and c) versus CH_4 (60) (in Fig. 3(ii)b and c) molecules occur. For CO_2, the six adsorption sites are retained around the pore periphery. However, the intensity in the central pore region as observed in NG system is diminished, as evidenced by comparison between Fig. 3(i)a, b and c. With diminishing intensity in the pore center, six moderate to high intensity sites begin to arise outside the pores and also in the intercrystalline gaps. This behavior agrees with our previously reported study [90]. While retention of the six adsorption sites at the pore periphery and additional sites in the inter-crystalline space at the expense of the pore center intensity is seen in both LCG and IG_OD-0, the new additional sites seem to be stronger in IG_OD-0. This is because the crystallite size is larger while the intercrystalline space is smaller in LCG. In contrast to CO_2, for CH_4 no significant migration of molecules is observed, with the introduction of intercrystalline spacing in LCG and IG_OD-0 systems (Fig. 3(ii) a, b and c). The CH_4 molecules are adsorbed relatively more homogenously, and a few can be found in the inter-crystalline space between adjacent pores, suggesting the absence of strong adsorption sites. With the introduction of OD accompanied with intercrystalline spacing, in system IG_OD-10 CO_2 molecules appear to follow the reoriented center crystallite. The CO_2 molecules continue to be regularly distributed along the strong adsorption sites, as observed in IG_OD-0 system. With the introduction of OD, no significant change in these sites is observed. However, a moderate increase in intensity of CO_2 molecules is observed in the intercrystalline spacing. This distribution is further confirmed in the intensity maps along XZ and YZ – axis, shown in the supplemental Figs. S1(i) and S2(i), respectively. Similarly, CH_4 molecules are mainly distributed around the Mg-MOF-74 pores, with no considerable influence of OD. With further increase in OD both CO_2 and CH_4 molecules continue to redistribute as a function of the OD value. Overall, with the introduction of intercrystalline spacing and OD CO_2 molecules form new adsorption sites around the periphery of pores and within the intercrystalline spacing. Conversely, the CH_4 molecule are mainly distributed around the pores and are absent in the intercrystalline gaps, an important consideration for industrial application and separation of the two gases [1,2,4].

In Fig. 3(ii)(a) for NG and (b) for LCG system the empty space at x =

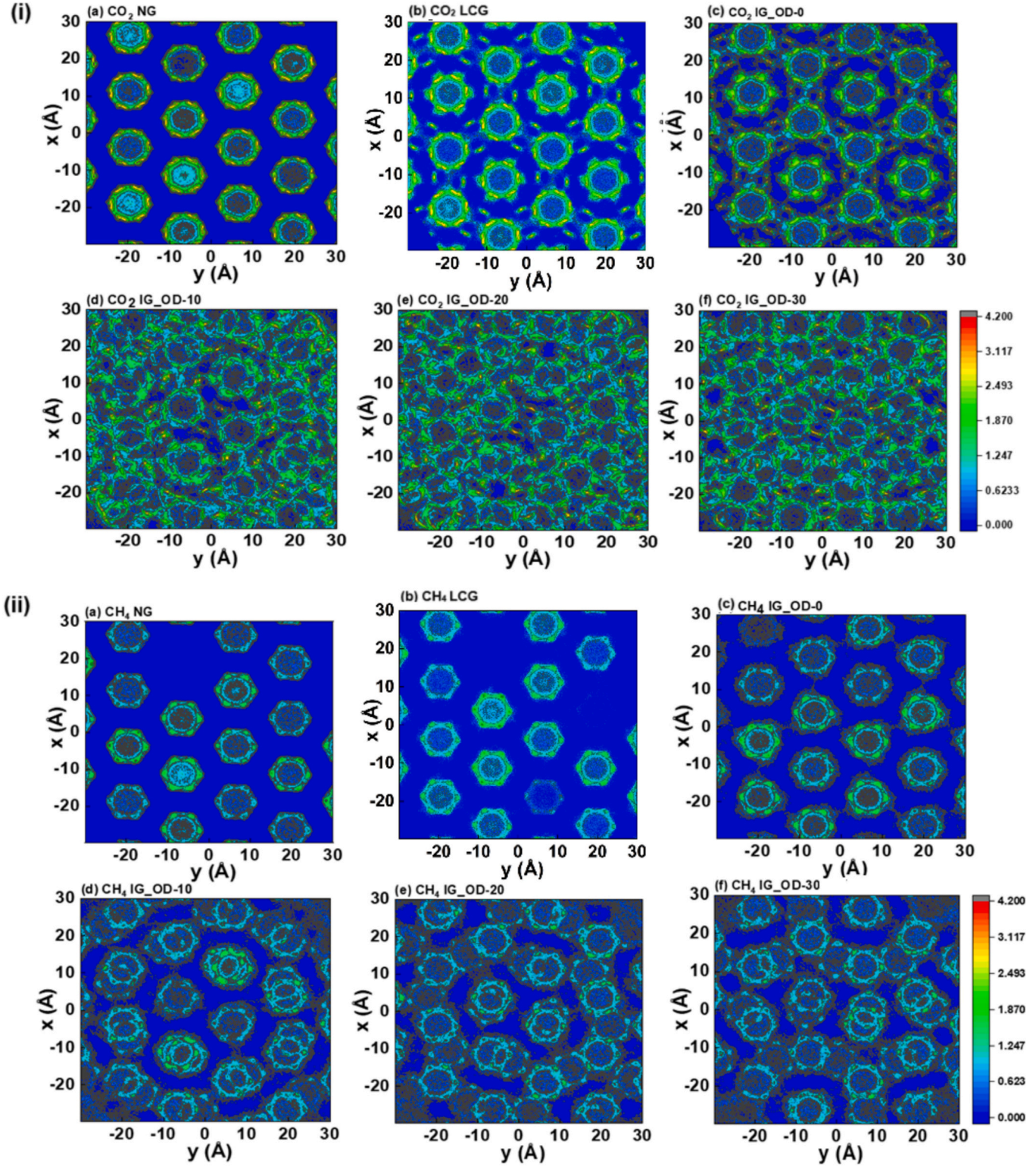

Fig. 3. Distribution of (i) 510 Carbon atoms of CO_2 molecules and (ii) 60 Carbon atoms of CH_4 molecules in the X − Y plane, for (a) NG, (b) LCG, (c) IG_OD-0, (d) IG_OD-10, (e) IG_OD-20 and (f) IG_OD-30 in Mg-MOF-74. The *Z*-intensity depicts the value log (N + 1), with N corresponding to the number of CO_2 or CH_4 molecules occupying a specific location at some instant during the whole production run time of 5 ns made up of 10,000-time frames.

20 Å and y = −10 Å and x = 10 Å and y = 20 Å values, respectively, corresponds to the absence of the CH_4 molecules. Pores in NG are isolated from each other. This means that while molecules are free to move within a pore, they cannot migrate between different pores. Thus, a pore that does not have an adsorbed molecule at $t = 0$, will remain vacant throughout the simulation. Equivalently the molecules are expected to be stuck in the pores in which they started, perpetually, without being able to diffuse to other pores. For CH_4 the total number of adsorbed molecules being relatively low, the probability of a pore remaining vacant when the molecules are randomly distributed is non-negligible. While for systems with inter-crystalline space the pores are no longer isolated, the inter-pore migration might still be subject to a potential

barrier, making it difficult. This could result in a pore that remains vacant throughout the simulation in Fig. 3 (ii) (b).

3.3. Orientation distribution

We calculated the orientation distribution function (ODF) $g(\theta)$ of CO_2 molecules along X-, Y- and Z- axis by counting the number of molecules that have their molecular axis making an angle θ with a Cartesian axis at any given time. Thus, the function $g(\theta)$ was calculated using the following expression

$$g(\theta) = \frac{1}{NN_t}\sum_{i}^{N}\sum_{j}^{N_t}\delta(\theta_{i,j} - \theta) \tag{3}$$

here $\theta_{i,j}$ is the angle made by the molecular axis of the i^{th} CO_2 molecule with a given Cartesian axis in the j^{th} time frame. Averages are taken over both the number of CO_2 molecules N and the total number of time frames N_t.

For comparison, the theoretically calculated isotropic distribution is also shown in the Fig. 4. In the absence of a preferred orientation, the orientational distribution function is expected to be isotropic. This isotropic distribution would be proportional to $2\pi r\sin\theta$ for a molecule with radius of gyration r. Isotropic behavior of ODF exhibits a broad peak at around 90°. Any deviation of the ODF obtained from the simulations from the isotropic ODF indicates a preferred orientation. The ODF plots for NG, IG_OD-0 and IG_OD-5 systems are shown in Fig. 4(a), (a) and (c), respectively, while the complete set of ODF plots are shown in the supplemental Fig. S3.

For CO_2 molecules, the NG system ODF shows a behavior close to isotropic. This behavior results from the hexagonal geometry of MOF pores and the pore size being nearly four times larger as compared to the CO_2 molecules. This makes at least six different orientations probable for the adsorbed CO_2 molecules in the X – Y plane, and the infinite space along the Z – direction, therefore making the ODF behavior nearly isotropic. With the introduction of intercrystalline gaps in IG_OD-0 system, signatures of preferred orientation are observed along all the three X-, Y- and *Z*- directions. As a result, deviation from the isotropic behavior is observed in ODF (Fig. 4(b)). This behavior can be attributed to the exposed surfaces, favoring the orientation of CO_2 molecules with respect to X– and Y– axis, in addition to Z – axis. Rotating the middle crystallite by 5° with respect to the other crystallites coupled with intercrystalline spacing (Fig. 4(c)), the signatures of anisotropic behavior are retained along all three directions. Thereafter, no significant influence of orientational disorder is observed on ODF with the presence of anisotropic behavior. The ODF shown for IG_OD-5 system in Fig. 4(c) is representative for all the higher OD systems. Along z -axis the two maxima at ~45° and ~ 135° (equivalent molecular symmetry) persist. The appearance of these peaks most likely arises due to the presence of intercrystalline gaps, owing to their absence in NG system. We note that a preference of 45° inclination of CO_2 with respect to pore axis (*Z*-direction) has been observed in several studies on CO_2 confined in nanoporous silica too [101,102].

The anisotropy parameter (φ) is calculated to quantify the deviation from isotropic behavior. The anisotropy parameter or degree of anisotropy is defined as the root mean square deviation from isotropic behavior.

$$\varphi = \sqrt{\frac{1}{N}\sum_{i}^{N}\left(g_{iso}(\theta_i) - g_{mol}(\theta_i)\right)^2} \tag{4}$$

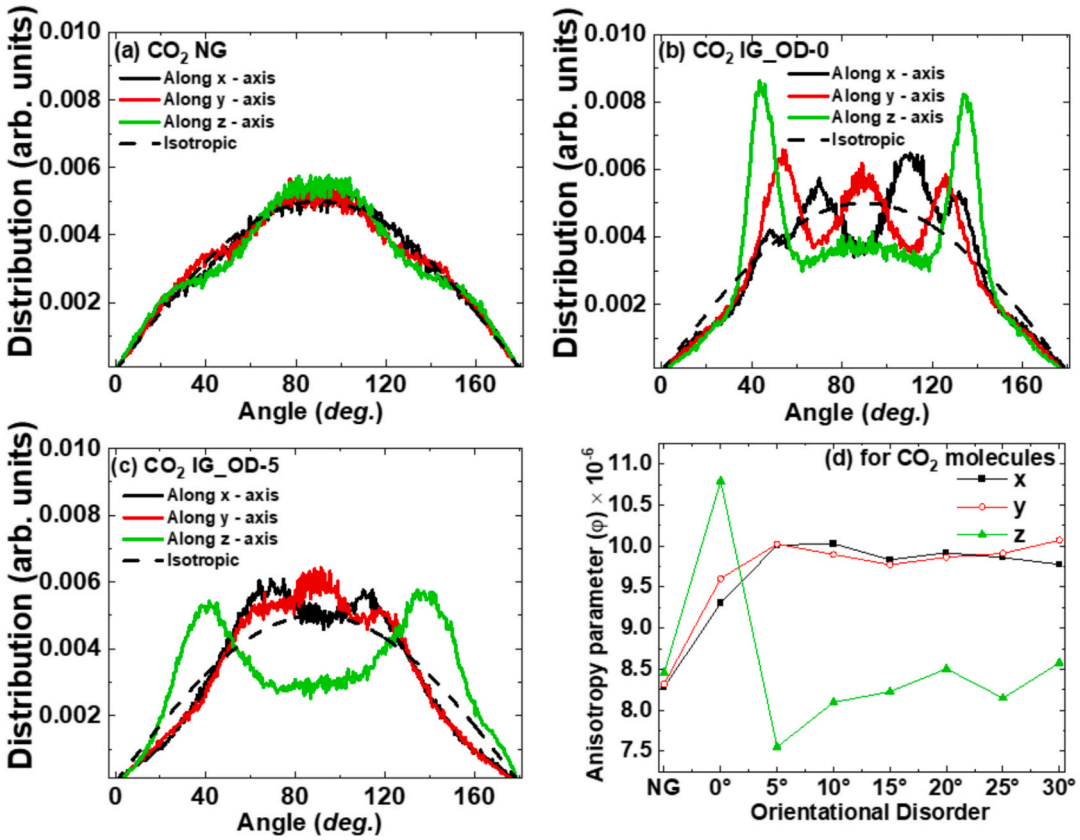

Fig. 4. Orientation distribution function (ODF) for CO_2 molecules along X-, Y- and Z- directions for (a) NG, (b) IG_OD-0, and (c) IG_OD-5 systems. The ODF for IG_OD-5 system in (c) is representative for all the higher OD systems. The broken line in the figures depicts the expected orientational distribution for an ideal isotropic system. (d) The anisotropy parameter (φ) as a function of orientation disorder for CO_2 molecules in Mg-MOF-74 system, along X–, Y– and Z– axis. φ values show the deviation from isotropic behavior, determined as a root mean square deviation from isotropic behavior. Lines serve as guide to the eye.

where g is the orientational distribution function and the subscripts *iso* and *mol* stand for the isotropic case and the observed case of CO_2 in Mg-MOF.

The corresponding plot of the anisotropy parameter (φ) as a function of orientational disorder along X-, Y- and *Z*- directions is shown in Fig. 4 (d). Generally, the larger the value of φ, the greater the deviation from isotropic behavior. As expected from the ODF, along the X- and Y- axis the anisotropy parameter exhibits an increase from NG up to 5° OD system with no significant change for higher rotations.

Interestingly, along the *Z*- direction, φ exhibits an increase between NG and IG_OD-0 system. This behavior reflects the presence of exposed surfaces with the introduction of IG of 5 Å. With the introduction of OD of 5° in IG_OD-5, the φ value along Z-direction exhibits a decrease as compared to 0° OD system. As a result of OD, the straight channel path along Z- axis is hindered and CO_2 molecular interactions with Mg^{2+} ions of neighboring MOFs are weakened. This leads to a reduction in φ value at 5° OD. With further increase in OD from 5° up to 30°, φ exhibits a slight increase. This may occur due to an increase in the electrostatic interaction of the surrounding MOF and CO_2 molecules with Mg^{2+} ions. This is further detailed and discussed later in Fig. 8.

3.4. Translation dynamics

To understand the translation diffusive motion of CO_2 and CH_4 molecules in Mg-MOF-74, time dependent mean square displacement (MSD) of the center of mass of the molecules is calculated.

Fig. 5 shows time dependent overall MSD as a function of orientational disorder for (a) CO_2 and (b) CH_4 molecules. Linear dependence of MSD with time is observed for both CO_2 and CH_4 molecules at all the OD values indicating normal diffusion. Interestingly, for CO_2 molecules MSD in Fig. 5(a) initially shows a decrease between NG and 0° OD system, behavior associated with the exposed surfaces resulting from the intercrystalline spacing in 0° OD system. These exposed surfaces may lead to strong adsorption of CO_2, therefore reducing the MSD. The introduction of 5° OD and increase in its value up to 15° leads to a continuous increase in MSD values. Further increase in OD from 15° to 25°, produces a decreasing MSD trend again, correlated with the possibility that the opposing MOF surfaces begin to realign (Schematic in Fig. 8).

The directional dependent MSD as a function of time for CO_2 molecules along X-, Y- and *Z*- axis is shown in Fig. S4. For NG and 0° OD systems, the MSD along Z- direction exhibits higher values compared to the MSD along X- and Y- directions. The difference between Z-direction and X-, Y- direction is reduced for 0° OD system, as compared to NG system. The introduction of intercrystalline spacing in 0° OD system facilitates the movement of CO_2 molecules along both X- and Y- direction, in addition to Z- direction.

Contrasting behavior for CH_4 molecules is observed in MSD shown in Fig. 5(b). Initially there is a very minor influence of intercrystalline spacing with increase in MSD between NG and 0° OD systems. This may imply that CH_4 molecules do not show strong adsorption on the surface in contrast to the behavior observed for CO_2 molecules. However, with the introduction of 5° OD an increase in MSD value is observed.

The diffusion coefficients are obtained by fitting the time dependent MSD using Einstein relation. The fitting is performed for the time scales beyond 100 ps (approx.), much above the ballistic region which lasts for only a few picoseconds. The diffusion coefficients as a function of OD for CO_2 and CH_4 molecules in Mg-MOF-74 are shown in Fig. 6(a) and (b), respectively.

Overall, the diffusion coefficient for CO_2 molecules (shown in Fig. 6 (a)) exhibits a decrease from NG to 0° OD, an increase from 0° up to 15° OD, decreasing again from 15° up to nearly 25° OD. This is in corroboration with the MSD behavior in Fig. 5. As expected, this behavior is nearly replicated in the diffusion coefficient along the Z-axis. While along X- and Y- axis, it is observed that diffusion coefficients exhibit slight increase up to 5° OD and remain nearly unchanged thereafter.

The diffusion coefficients for CH_4 molecule are shown in Fig. 6(b). The diffusion coefficients exhibit an increase from NG up to 5° OD system. This may be caused by volume increase of the simulation unit cell. When the orientational disorder is introduced in 5° to 30° system, to accommodate the rotation of the crystallites (based on IG OD-30 system), the simulation cell volume is increased. The simulation cell volume is increased between 0° – 5°, and is fixed thereafter. This may have an influence on the diffusion of CH_4 molecules, where for 0° system the volume is lower as compared to the 5° system. We see no influence of this on CO_2 molecules, which may be ascribed to the strong affinity of CO_2 and Mg^{2+} ions of Mg-MOF-74. Similar trends in all the directional diffusion coefficient values as a function of OD are observed.

Further, we calculated the mean square displacement of CO_2 and CH_4 molecules in different regions (crystallite and inter-crystalline space) for IG_OD-0 system. As compared to the NG system (shown in Fig. 5a), the reduction in MSD for IG_OD-0 system can be ascribed to the introduced intercrystalline spacing. Since the intercrystalline spacing forms the exposed surfaces, favoring the strong adsorption of CO_2 and in turn reducing the MSD. This is also confirmed in Fig. S7, wherein the MSD in the intercrystalline gaps is smaller than the ones present in the crystallites. This is also reflected in the obtained value of diffusion coefficients, for molecules within the crystallites (22.9 (7) $\times$ 10^{-10} m^2/s) and for those in the gaps (13.7 $\times$ 10^{-10} m^2/s). For comparison, we also calculated the MSD of CH_4 molecule for IG_OD-0 system. No significant difference between the MSDs for molecules with the crystallites or gaps is observed.

3.5. Rotational dynamics

To explore the rotational dynamics behavior of CO_2 molecules as a function of OD, rotational correlation function (RCF; $C_R(t)$) is calculated. The corresponding equation is shown below,

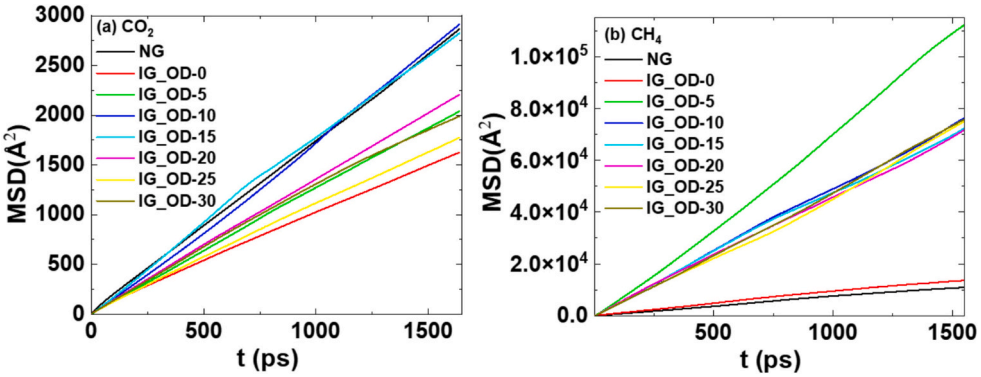

Fig. 5. Time dependent mean square displacement (MSD) as a function of OD for (a) CO_2 and (b) CH_4 molecules in Mg-MOF-74.

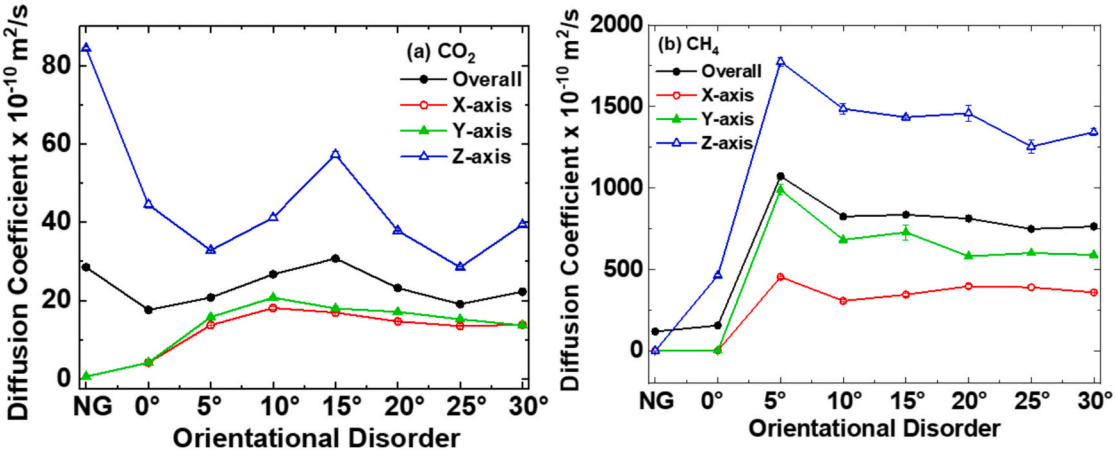

Fig. 6. Diffusion coefficient of (a) CO_2 and (b) CH_4 molecules for overall and along X-, Y- and *Z*-direction MSD as a function of OD. The diffusion coefficient is obtained by fitting the MSD using Einstein relation beyond 100 ps (approx.) time scales. The error bars are smaller than symbol size. Lines serve as guide to the eye.

$$C_R(t) = \langle \boldsymbol{u}(t+t_0).\boldsymbol{u}(t_0) \rangle \quad (5)$$

where, $\boldsymbol{u}$ is a unit vector attached to the molecular axis and, angular brackets $\langle\rangle$ indicate an ensemble average taken over all molecules and time origin t_0. Experimentally, RCF is related to the dipole correlation function, which can be obtained from dielectric and/or infra-red spectroscopy measurements.

The calculated RCF as a function of time for all OD conditions is shown in Fig. 7. For the NG system relatively faster decay is observed, indicating the faster rotation of CO_2 molecules in the absence of intercrystalline spacing and OD. At a longer timescale of around 100 ps (approx.) the RCF decays completely to zero, suggesting that a CO_2 molecule spans the entire orientational space within this time. With the induced intercrystalline spacing and the absence of OD for 0° OD system (IG_OD-0), relatively slower decay of RCF is observed as compared to NG system. The introduction of 5° OD (IG_OD-5) leads to further reduction in the decay rate of RCF, implying further hindrance to the rotational motion of CO_2 molecules with induced OD. However, the difference in the rate of reduction is significantly smaller as compared to the one between NG and 0° OD system. Moreover, the RCF in this system does not decay to zero during the entire simulation time, suggesting that a typical molecule does not exhaust all possible orientations within this time. This in turn would imply an avoidance of some orientations and preference for others by the molecule. Interestingly, further increase in OD causes slightly faster decay of RCF and no significant change in this behavior is observed with increasing OD. This behavior indicates very small (reduced hindrance to the rotational motion of CO_2 molecules) or no significant influence of OD on the rotational motion of CO_2 molecules.

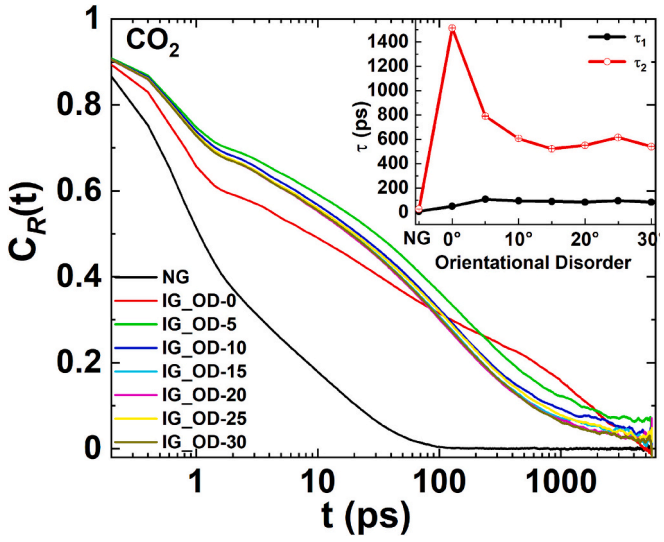

Fig. 7. The calculated rotational correlation function (RCF) for all the OD values. The RCF is calculated using eq. 5, given in the text. The inset depicts the rotational correlation times (τ_1 and τ_2) obtained by fitting the biexponential decay function to RCF above 1 ps (approx.).

Additionally, we also obtained the rotational time scales. A biexponential decay function is fitted to RCF above 1 ps, with rotational correlation times (τ_1 and τ_2) as the fitting parameters. The corresponding rotational correlation times (τ_1 and τ_2) as a function of OD are shown in the inset to Fig. 7. In accordance with RCF shown in Fig. 7, initially the τ_2 value exhibit an increase from NG to 0° OD with indicating slower rotation due to introduction of inter-crystalline space. Further change in OD leads to relatively milder but systematic change in the rotational time scales mirroring the trend seen in the translational motion.

4. Discussion

Mg-MOF-74 framework is reported to be one of most promising candidates for CO_2 adsorption, both experimentally and theoretically. Strong electrostatic interaction with Mg ion is responsible for the high affinity of this material to CO_2 adsorption [78]. This suggests that Mg-MOF-74 may be able to selectively adsorb quadrupolar CO_2 from a binary mixture with a non-polar fluid like methane [103,104]. In a recent computational study, Zhang et al. [105] demonstrated the enhancement of selective adsorption of CO_2 over CH_4 from a binary mixture via functionalization of Mg-MOF-74. Functionalization of Mg-MOF-74 with groups -O-Li, -NH_2 and -SH were found to enhance the selectivity. In a previous publication, we found that inserting intercrystalline space in Mg-MOF-74 resulted in additional strong adsorption sites for CO_2 on crystallite surfaces [90]. Because the interaction of CO_2 with new sites is predominantly electrostatic, these sites will discriminate between quadrupolar CO_2 and a non-polar molecule like CH_4. Our work indicates that the newly exposed adsorption sites for CO_2 on the crystallite surfaces (IG_OD-0) add to the selective adsorption thereby enhancing the selectivity of CO_2 by a factor of ~1.5 and up to ~2 when the middle crystallite is rotated. At 1 atm (= 101.325 kPa), this enhancement in selectivity is like that obtained by functionalizing the adsorbent by -O-Li groups.

The enhancement in selectivity due to disorder is a result of additional adsorption sites selectively favorable for CO_2 because of its quadrupole moment that exhibit strong electrostatic interactions. A molecule with a quadrupole moment is governed by spatial distribution of its partial charges. This in turn may make the molecule sensitive to the

addition of electronegative or inductive moieties, particularly around the periphery. CO_2 is a linear molecule with no dipole, but finite quadrupole moment. The presence of strong interactions with quadrupole moment of CO_2, also leads to increase in the diffusivity of confined hydrocarbons with the addition of CO_2 molecules [106,107]. While this study focused on a mixture of CO_2 with CH_4, we suggest that the results obtained here should be useful for more general mixtures of CO_2 with other non-polar fluids.

While adding OD by rotating the middle crystallites does not lead to a significant change in the adsorption selectivity beyond a rotation of 5°, structural and dynamical properties of CO_2 exhibit a stronger dependence on the extent of rotation of the middle crystallite. For the system without intercrystalline spacing and orientational disorder (i. e., NG), six strong adsorption sites around the periphery of MOF (bright yellow regions in Fig. 3(i)) are observed, combined with a few CO_2 molecules adsorbed in the pore center. In contrast, for CH_4 molecules this difference of strong absorption site is not so prominent, can be ascribed to the lower number of CH_4 molecules to begin with. With the introduction of intercrystalline spacing (i. e., in IG_OD-0), the CO_2 molecules begin to occupy the intercrystalline spacing close to the outer periphery of Mg-MOF-74. This is in addition to the previously occupied six sites (in NG) around the Mg-MOF-74 periphery within the pores. These newly available strong sites (outer periphery of Mg-MOF-74 pores) of adsorption for CO_2 hinder both translational and rotational motion as observed in Figs. 6 and 7. Conversely, CH_4 molecules largely prefer to stay within the pore volume of Mg-MOF-74. With the introduction of OD, the interaction between CO_2 molecules and Mg^{2+} ions of Mg-MOF-74 system goes through the cycle of weakening (from OD of 5° up to 15°) and strengthening (from OD of 15° up to 25°). Unlike CO_2, no significant influence of OD is observed on CH_4 molecules, which are distributed uniformly around the Mg-MOF-74 pores.

A 2D representation of CO_2 adsorption in Mg-MOF-74 system including the interaction with Mg^{2+} ions as a function of orientational disorder (OD) is shown in Fig. 8. The figure also shows the pair distribution function between Mg ion and atoms of CO_2 for three representative systems, while the functions for all systems are included in the supplementary information (Fig. S9). The electropositive Mg ion in Mg-MOF-74 attracts the electronegative oxygen atom in the CO_2 molecule providing strong adsorption sites for the latter. This is evident from the positioning of the first pair distribution function peak for the pair Mg—O (oxygen of CO_2) that occurs at shorter distances compared to the peak in the Mg—C (carbon of CO_2) pair distribution function. With the introduction of OD, the guest host interactions exhibit changes as evident from both the position and the strength of peaks in the pair distribution functions. The peak intensity of the pair distribution for both pairs increases because of the additional adsorption sites that appear in the inter-crystalline region. A typical Mg ion now has a larger coordination number with both the atoms of CO_2 because of these additional sites. In addition, the Mg—C pair now has a slightly larger interatomic distance (position of first peak) while the Mg—O pair distance decreases. When the middle crystallite is rotated the peak position for Mg—C shifts again, this time towards smaller distances, while the Mg—O distance decreases further. Also, the intensity of the peaks in the pair distribution function increases on rotating the crystallite. This is because the rotation of the middle crystallite makes an additional site on the opposite crystallite available for pairing. To explain this, we refer to the schematic shown in the left part of Fig. 8. The hexagonal MOF pores are represented in blue and position of four Mg^{2+} ions are marked as A, B, C, and D. For IG_OD-

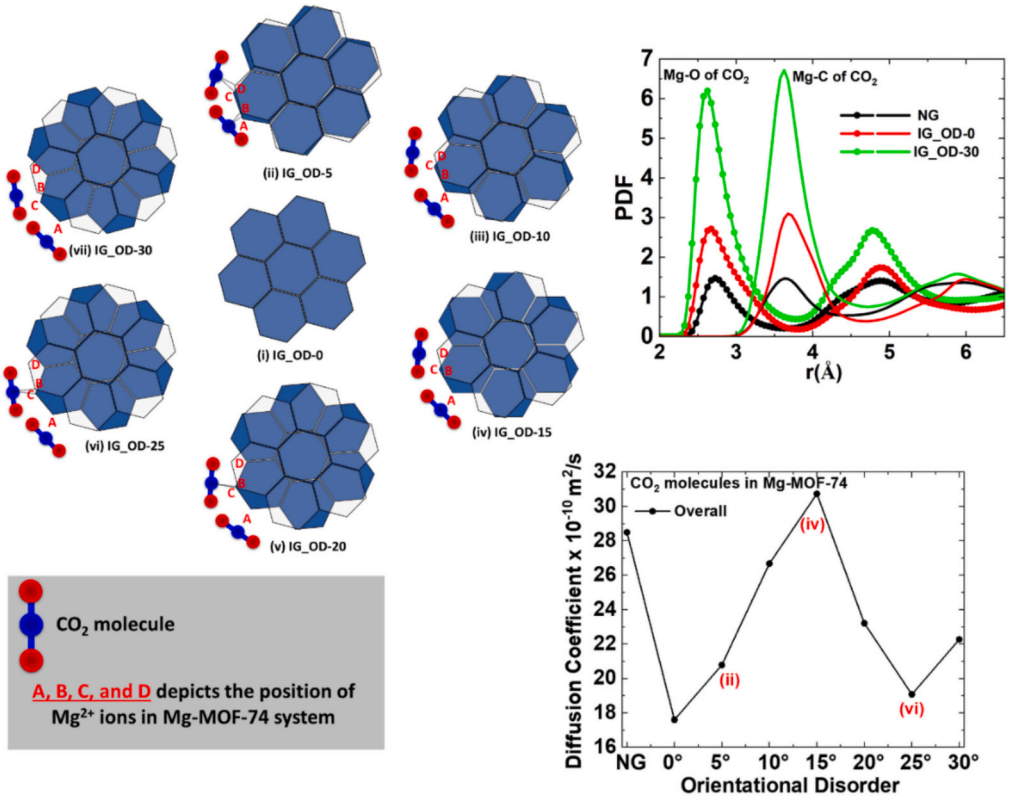

Fig. 8. A 2D schematic representation of CO_2 adsorption in Mg-MOF-74 system, the interaction with Mg^{2+} ions as a function of orientational disorder (OD). The hexagonal MOF pores are represented in blue. Points marked as A, B, C, D represent the location of Mg^{2+} ions in Mg-MOF-74 system. (i) IG_OD-0, (ii) for IG_OD-5, (iii) IG_OD-10, (iv) IG_OD-15, (v) IG_OD-20, (vi) IG_OD-25 and, (vii) IG_OD-30 system. The top right figure shows the pair distribution function (PDF) for NG, IG_OD-0 and IG_OD-30. The overall behavior of diffusion coefficient as a function of OD shown in the bottom left is explained using this simple (average) schematic with the misalignment and re-alignment of Mg^{2+} ions position marked as A, B, C, D with respect to the CO_2 molecules. (For interpretation of the references to colour in this figure legend, the reader is referred to the web version of this article.)

0 system (Fig. 8(i)), in the absence of OD, CO_2 is adsorbed on the surface, with highly restrictive diffusion. The points A, B, C, and D coincide in this case (not shown in the Fig. 8(i)). With the introduction of OD of 5° in IG_OD-5 (Fig. 8(ii)), the point pairs A-B and C—D begin to separate, creating a distance between CO_2 molecules and Mg^{2+} ions (i. e., point B and D). This may cause the weakening of $Mg^{2+} - CO_2$ interactions, and hence increase in diffusion coefficient. With further increase in OD up to 15° (in Fig. 8(iii) and (iv)) the distance increases between CO_2 molecules and Mg^{2+} ions (at point B and D). This favors further reduction in the diffusion coefficient of CO_2 molecules. Interestingly, at the same time with increasing OD up to 15° the points B and C begin to align to each other. At OD values of 20° and 25° (in Fig. 8(v) and (vi), respectively), the Mg^{2+} ions at point B and C come close enough to strengthen the interaction between CO_2 molecules and Mg^{2+} ions. This results in a decrease in diffusion coefficient value for CO_2 molecules. Further increase in OD to 30° for IG_OD-30 system (Fig. 8(vii)), the Mg^{2+} ions again start to separate at points B and C, leading to increase in the CO_2 diffusion coefficient. In contrast, for CH_4 molecules no significant influence of OD in MSD is observed. The large jump observed in diffusion coefficient between 0° and 5° OD system may be attributed to and associated with the redistribution of CO_2 molecules. Further, the diffusion coefficients obtained for CH_4 are nearly two orders of magnitude greater as compared to CO_2 molecules. The diffusion coefficients of CO_2 molecules exhibit good agreement with our previously reported studies in MOF with pure CO_2 system (S2 system and 20 mpuc loading) [90]. Our values are comparable with the values reported by Bendt et al. and by Krishna et al. [99].The rotational motion of CO_2 molecules is also influenced by addition of disorder. Initially, the introduction of intercrystalline spacing produces exposed surfaces that hinder the rotational motion of CO_2 molecules. The hindrance to rotation at longer times however, decreases significantly when the middle crystallite is rotated while the short time scale rotation continues to slow down for IG_OD-5 system, with no considerable change thereafter with increasing OD.

There is value in understanding the relationship of structural disorder, which may be in the form of orientational disorder (as in the present work) and/or structural defects, with the adsorption properties of the adsorbent (for example, Mg-MOF-74 in our case here). This is not only crucial for the development of higher quality adsorbent materials, but also for exploiting these structural disorders to improve and enhance the functionality of the adsorbent material. Computational work in this area is highly useful, because it is rather difficult to perform these kind of studies experimentally. The systematic variation and classification of orientation disorder could be extremely challenging in real materials, wherein the several kinds of structural disorder and/or defects are often present simultaneously. As the work reported here demonstrates, disorder in Mg-MOF-74 has significant effects on its performance in separating a mixture of CO_2 with CH_4 via selective adsorption. The property that makes this possible is the quadrupole moment of CO_2 and its electrostatic interaction with the Mg^{2+} ions. Therefore, it can be inferred that the gain in selectivity observed upon addition of disorder, orientational or otherwise, should be a general phenomenon for a mixture of CO_2 with a non-polar fluid. While OD in Mg-MOF-74 is found to have a rather weak effect on the adsorption and rotation of CO_2, its effect on the translational motion of CO_2 is significant and follows a systematic pattern that is dictated by the interplay of the pore geometry of Mg-MOF-74 and Mg^{2+}-CO_2 interactions. This systematic pattern can be utilized to tailor Mg-MOF-74 adsorbents with desired transport properties of confined CO_2. For example, consistent efforts have been recently directed towards the fabrication of oriented polycrystalline MOF superstructures [108]. Our study can help these efforts by providing the structure -property relations that could improve the performance of these materials. We note that while this study explores the effects of disorder in the adsorbent, the disorder introduced in this work has a systematically regular variation. In a real material, it would be challenging to (i) introduce disorder in such a regular manner, and (ii) maintain the width of the inter-crystalline space. The disorder in a real material will thus have a more complex effect on the properties of adsorbed fluids. The current simulation work is a first step in understanding these effects.

5. Conclusion

Molecular-level simulations demonstrate the overall influence of induced OD in Mg-MOF-74 on the separation of CO_2 and CH_4 gas mixture via selective adsorption. Disorder is introduced in the adsorbent by inserting intercrystalline space between adjacent crystallites and by rotating one crystallite with respect to others. Overall, we observe that Mg-MOF-74 can be a good candidate for the gas separation of CO_2 from CH_4 in gas mixture for industrial application. The separation capability of Mg-MOF-74 can be further enhanced by a factor of ~1.5–2 by introducing positional and orientational disorders. This enhancement is a result of additional adsorption sites selectively favorable for CO_2 due to its quadrupole moment that exhibit strong electrostatic interactions. Change in the structural and dynamical properties of the adsorbed species on introducing OD in the material is found to follow a systematic pattern dictated by the interplay of the pore geometry of Mg-MOF-74 and $Mg^{2+} - CO_2$ interactions. While this study focused on a mixture of CO_2 with CH_4, we suggest that the results obtained here should be useful for more general mixtures of CO_2 with other non-polar fluids. The obtained systematic results guide how to tailor Mg-MOF-74 with desired properties by purposeful introduction of OD.

Funding

This work received no external funding.

CRediT authorship contribution statement

I. Dhiman: Writing – review & editing, Writing – original draft, Visualization, Validation, Supervision, Software, Resources, Project administration, Methodology, Investigation, Formal analysis, Data curation, Conceptualization. **David R. Cole:** Writing – review & editing. **Siddharth Gautam:** Writing – review & editing, Writing – original draft, Visualization, Validation, Supervision, Software, Resources, Project administration, Methodology, Investigation, Formal analysis, Data curation, Conceptualization.

Declaration of competing interest

The authors declare that they have no known competing financial interests or personal relationships that could have appeared to influence the work reported in this paper.

Acknowledgements

We would like to acknowledge STFC's Daresbury Laboratory for providing the package DL-Poly, which was used in this work. Help received in the analysis of MD simulations from the visualization packages VESTA and VMD is also acknowledged. I. D. acknowledges KIFÜ for awarding the access to computational resources based in Hungary at Budapest.

Appendix A. Supplementary data

Supplementary data to this article can be found online at https://doi.org/10.1016/j.chemphys.2025.112661.

Data availability

All data supporting the findings reported in this work are included in the article and the associated supplementary information file.

References

[1] R.T. Yang, Gas Separation by Adsorption Processes 1, Singapore, World Scientific, 1997.
[2] H. Wang, D. Luo, E. Velasco, L. Yu, J. Li, Separation of alkane and alkene mixtures by metal–organic frameworks, J. Mater. Chem. A 9 (2021) 20874–20896.
[3] T.F. Stocker, D. Qin, G.-K. Plattner, M. Tignor, S.K. Allen, J. Boschung, A. Nauels, Y. Xia, V. Bex, P.M. Midgley, IPCC (Eds.), Climate change 2013: The physical science basis. Contribution of working group I to the fifth assessment report of the intergovernmental panel on climate change; Stocker, (Eds.); Cambridge University Press: Cambridge, UK; New York, NY, USA, **2013**; p. 1535, 2013.
[4] T.R. Anderson, E. Hawkins, D.J. Philip, CO_2, the Greenhouse Effect and Global Warming: From the Pioneering Work of Arrhenius and Callendar to today's Earth System Models. *Endeavour* **2016**, 40, 178–187. Kerry, F.G. Industrial Gas Handbook: Gas Separation and Purification, CRC Press, Boca Raton, FL, USA, 2007.
[5] R.S. Haszeldine, Carbon capture and storage: how green can black be? Science 325 (2009) 1647–1652.
[6] T.R. Karl, K.E. Trenberth, Modern global climate change, Science 302 (2003) 1719–1723.
[7] C.D. Keeling, T.P. Whorf, M. Wahlen, J. Vanderplicht, Interannual extremes in the rate of rise of atmospheric carbon dioxide since 1980, Nature 375 (1995) 666–670.
[8] E. Kintisch, Making dirty coal plants cleaner, Science 317 (2007) 184–186.
[9] J.L. Zhu, Y.H. Wang, J.C. Zhang, Experimental investigation of adsorption of NO and SO_2 on modified activated carbon sorbent from flue gases, Energy Covers. Manage. 46 (2005) 2173.
[10] X.C. Xu, C.H. Chen, H.Y. Qi, Development of coal combustion pollution control for SO_2 and NO_x in China, Fuel Process. Technol. 62 (2000) 153.
[11] H.Q. Yang, Z.H. Xu, M.H. Fan, Progress in carbon dioxide separation and capture: a review, J. Environ. Sci. 20 (2008) 14.
[12] E.S. Rubin, H. Mantripragada, A. Marks, P. Versteeg, J. Kitchin, The outlook for improved carbon capture technology, Prog. Energy Combust. Sci. 38 (2012) 630–671.
[13] D.Y.C. Leung, G. Caramanna, M.M. Maroto-valer, An overview of current status of carbon dioxide capture and storage technologies, Renew. Sust. Energ. Rev. 39 (2014) 426–443.
[14] J.C.M. Pires, F.G. Martins, M.C.M. Alvim-Ferraz, M. Simões, Recent developments on carbon capture and storage: an overview, Chem. Eng. Res. Des. 89 (2011) 1446–1460.
[15] S. Faramawy, T. Zaki, A.A.E. Sakr, Natural gas origin, composition, and processing: a review, J. Nat. Gas Sci. Eng. 34 (2016) 34–54.
[16] N. Abatzoglou, S. Boivin, A review of biogas purification processes, Biofuels Bioprod. Biorefin. 3 (2009) 42–71.
[17] R.M. Cuéllar-Franca, A. Azapagic, Carbon capture, storage and utilisation technologies: a critical analysis and comparison of their life cycle environmental impacts, J. CO2 Util. 9 (2015) 82–102.
[18] H. Coninck, de; Benson, S. M., Carbon dioxide capture and storage: issues and prospects, Annu. Rev. Environ. Resour. 39 (2014) 243–270.
[19] R. Gunderson, D. Stuart, B. Petersen, The fossil fuel industry's framing of carbon capture and storage: faith in innovation, value instrumentalization, and status quo maintenance, J. Clean. Prod. 252 (2020) 119767.
[20] IEA, https://data.worldbank.org/indicator/eg.use.comm.fo.zs (n. d.).
[21] A. Samanta, A. Zhao, G.K.H. Shimizu, P. Sarkar, R. Gupta, Post-combustion CO_2 capture using solid sorbents: a review, Ind. Eng. Chem. Res. 51 (2012) 1438–1463.
[22] M.B. Kermani, A. Morshed, Carbon dioxide corrosion in oil and gas production: a compendium, Corrosion 59 (8) (2003) 659–683.
[23] M.T. Kallo, M.J. Lennox, Understanding CO_2/CH_4 separation in pristine and defective 2D MOF CuBDC Nanosheets via nonequilibrium molecular dynamics, Langmuir 36 (2020) 13591–13600.
[24] D.M. D'Alessandro, B. Smit, J.R. Long, Carbon dioxide capture: prospects for new materials Angew, Chem. Int. Ed. 49 (2010) 6058–6082.
[25] K. Sumida, D.L. Rogow, J.A. Mason, T.M. McDonald, E.D. Bloch, Z.R. Herm, T. H. Bae, J.R. Long, Carbon dioxide capture in metal-organic frameworks, Chem. Rev. 112 (2012) 724–781.
[26] R.S. Haszeldine, Carbon capture and storage: how green can black be? Science 325 (2009) 1647–1652.
[27] D.M. Ruthven, Principles of Adsorption and Adsorption Processes; John Wiley & Sons: Hoboken, NJ, USA, 1984.
[28] R. Serna-Guerrero, E. Dana, A. Sayari, New insights into the interactions of CO_2 with amine-functionalized silica, Ind. Eng. Chem. Res. 47 (2008) 9406–9412.
[29] J.C. Hicks, J.H. Drese, D.J. Fauth, M.L. Gray, G. Qi, C.W. Jones, Designing adsorbents for co_2 capture from flue gas -hyperbranched aminosilicas capable of capturing CO_2 reversibly, J. Am. Chem. Soc. 130 (2008) 2902–2903.
[30] G.P. Knowles, S.W. Delaney, A.L. Chaffee, Diethylenetriamine[propyl(silyl)]-functionalized (DT) mesoporous silicas as CO_2 adsorbents, Ind. Eng. Chem. Res. 45 (2006) 2626–2633.
[31] E. Berger, M.W. Hahn, T. Przybilla, B. Winter, E. Spiecker, A. Jentys, J.A. Lercher, Impact of solvents and surfactants on the self-assembly of nanostructured amine functionalized silica spheres for CO_2 capture, J. Energy Chem. 25 (2016) 327–335.
[32] M.W. Hahn, J. Jelic, E. Berger, K. Reuter, A. Jentys, J.A. Lercher, Role of amine functionality for CO_2 chemisorption on silica, J. Phys. Chem. B 120 (2016) 1988–1995.
[33] G.S. Foo, J.J. Lee, C.-H. Chen, S.E. Hayes, C. Sievers, C.W. Jones, Elucidation of surface species through in-situ FTIR spectroscopy of carbon dioxide adsorption on amine-grafted SBA-15, ChemSusChem 10 (2017) 266–276.
[34] A. Goj, D.S. Sholl, E.D. Akten, D. Kohen, Atomistic simulations of CO_2 and N_2 adsorption in silica zeolites: the impact of pore size and shape, J. Phys. Chem. B 106 (2002) 8367–8375.
[35] R.V. Siriwardane, M.-S. Shen, E.P. Fisher, Adsorption of CO_2, N_2, and O_2 on natural zeolites, Energy Fuel 17 (2003) 571–576.
[36] R.V. Siriwardane, M.-S. Shen, E.P. Fisher, J. Losch, Adsorption of CO_2 on zeolites at moderate temperatures, Energy Fuel 19 (2005) 1153–1159.
[37] Z. Liang, M. Marshall, A.L. Chaffee, CO_2 adsorption-based separation by metal organic framework (cu-BTC) versus zeolite, Energy Fuel 23 (2009) 2785–2789.
[38] F. Su, C. Lu, S.-C. Kuo, W. Zeng, Adsorption of CO_2 on amine-functionalized Y-type zeolites, Energy Fuel 24 (2010) 1441–1448.
[39] M.R. Hudson, W.L. Queen, J.A. Mason, D.W. Fickel, R.F. Lobo, C.M. Brown, Unconventional, highly selective CO_2 adsorption in zeolite SSZ-13, J. Am. Chem. Soc. 134 (2012) 1970–1973.
[40] J. Kim, L.-C. Lin, J.A. Swisher, M. Haranczyk, B. Smit, Predicting large CO_2 adsorption in aluminosilicate zeolites for postcombustion carbon dioxide capture, J. Am. Chem. Soc. 134 (2012) 18940–18943.
[41] C. Lu, H. Bai, B. Wu, F. Su, J.F. Hwang, Comparative study of CO_2 capture by carbon nanotubes, activated carbons, and zeolites, Energy Fuel 22 (2008) 3050–3056.
[42] F. Su, C. Lu, W. Cnen, H. Bai, J.F. Hwang, Capture of CO_2 from flue gas via multiwalled carbon nanotubes, Sci. Total Environ. 407 (2009) 3017–3023.
[43] M. Rahimi, J.K. Singh, D.J. Babu, J.J. Schneider, F. Müller- Plathe, Understanding carbon dioxide adsorption in carbon nanotube arrays: molecular simulation and adsorption measurements, J. Phys. Chem. C 117 (2013) 13492–13501.
[44] D.J. Babu, M. Bruns, R. Schneider, D. Gerthsen, J.J. Schneider, Understanding the influence of n-doping on the CO_2 adsorption characteristics in carbon nanomaterials, J. Phys. Chem. C 121 (2017) 616–626.
[45] D.J. Babu, J.J. Schneider, Gas adsorption studies of CO_2 in carbon nanomaterials: a case study of vertically aligned carbon nanotubes, Chem. Ing. Tech. 89 (2017) 1273–1287.
[46] Y. Li, R.T. Yang, Gas adsorption and storage in metal-organic framework MOF-177, Langmuir 23 (2007) 12937–12944.
[47] R. Banerjee, A. Phan, B. Wang, C. Knobler, H. Furukawa, M. O'Keeffe, O. M. Yaghi, High-throughput synthesis of zeolitic imidazolate frameworks and application to CO_2 capture, Science 319 (2008) 939–943.
[48] F. Salles, A. Ghoufi, G. Maurin, R.G. Bell, C. Mellot-Draznieks, G. Férey, Molecular dynamics simulations of breathing MOFs: structural transformations of mil-53(cr) upon thermal activation and CO_2 adsorption, Angew. Chem. Int. Ed. 47 (2008) 8487–8491.
[49] D. Britt, H. Furukawa, B. Wang, T.G. Glover, O.M. Yaghi, Highly efficient separation of carbon dioxide by a metal-organic framework replete with open metal sites, Proc. Natl. Acad. Sci. USA 106 (2009) 20637–20640.
[50] S. Couck, J.F.M. Denayer, G.V. Baron, T. Rémy, J. Gascon, F. Kapteijn, An amine-functionalized mil-53 metal-organic framework with large separation power for CO_2 and CH_4, J. Am. Chem. Soc. 131 (2009) 6326–6327.
[51] Z. Zhao, Z. Li, Y.S. Lin, Adsorption and diffusion of carbon dioxide on metal-organic framework (MOF-5), Ind. Eng. Chem. Res. 48 (2009) 10015–10020.
[52] L. Hamon, E. Jolimaître, G.D. Pirngruber, CO_2 and CH_4 separation by adsorption using cu-BTC metal-organic framework, Ind. Eng. Chem. Res. 49 (2010) 7497–7503.
[53] D. Saha, Z. Bao, F. Jia, S. Deng, Adsorption of CO_2, CH_4, N_2O, and N_2 on MOF-5, MOF-177, and zeolite 5A, Environ. Sci. Technol. 44 (2010) 1820–1826.
[54] L. Valenzano, B. Civalleri, S. Chavan, G.T. Palomino, C.O. Areán, S. Bordiga, Computational and experimental studies on the adsorption of CO, N_2, and CO_2 on mg-MOF-74, J. Phys. Chem. C 114 (2010) 11185–11191.
[55] W.L. Queen, M.R. Hudson, E.D. Bloch, J.A. Mason, M.I. Gonzalez, J.S. Lee, D. Gygi, J.D. Howe, K. Lee, T.A. Darwish, et al., Comprehensive study of carbon dioxide adsorption in the metal-organic frameworks M2(dobdc) (M = Mg, Mn, Fe, Co, Ni, Cu, Zn), Chem. Sci. 5 (2014) 4569–4581.
[56] E. Braun, A.F. Zurhelle, W. Thijssen, S.K. Schnell, L.-C. Lin, J. Kim, J. A. Thompson, B. Smit, High-throughput computational screening of nanoporous adsorbents for CO_2 capture from natural gas, Mol. Syst. Des. Eng. 1 (2016) 175–188.
[57] R. Chanajaree, T. Chokbunpiam, J. Kärger, S. Hannongbua, S. Fritzsche, Investigating adsorption- and diffusion selectivity of CO_2 and CH_4 from air on zeolitic imidazolate framework-78 using molecular simulations, Microporous Mesoporous Mater. 274 (2019) 266–276.
[58] J. Liu, P.K. Thallapally, B.P. McGrail, D.R. Brown, J. Liu, Progress in adsorption-based CO_2 capture by metal-organic frameworks, Chem. Soc. Rev. 41 (2012) 2308–2322.
[59] J. Yu, L.-H. Xie, J.-R. Li, Y. Ma, J.M. Seminario, P.B. Balbuena, CO_2 capture and separations using mofs: computational and experimental studies, Chem. Rev. 117 (2017) 9674–9754.
[60] Z.Y. Yeo, T.L. Chew, P.W. Zhu, A.R. Mohamed, S.P. Chai, Conventional processes and membrane technology for carbon dioxide removal from natural gas: a review, J. Nat. Gas Chem. 21 (3) (2012) 282–298.
[61] J.L.C. Rowsell, O.M. Yaghi, Metal−organic frameworks: a new class of porous materials, Microporous Mesoporous Mater. 73 (1–2) (2004) 3–14.
[62] H. Furukawa, K.E. Cordova, M. O'Keeffe, O.M. Yaghi, The chemistry and applications of metal-organic frameworks, Science 341 (6149) (2013) 1230444.
[63] P.Z. Moghadam, A. Li, S.B. Wiggin, A. Tao, A.G.P. Maloney, P.A. Wood, S. C. Ward, D. Fairen-Jimenez, Development of a Cambridge structural database

subset: a collection of metal- organic frameworks for past, present, and future, Chem. Mater. 29 (7) (2017) 2618–2625.
[64] C.E. Wilmer, M. Leaf, C.Y. Lee, O.K. Farha, B.G. Hauser, J.T. Hupp, R.Q. Snurr, Large-scale screening of hypothetical metal-organic frameworks, Nat. Chem. 4 (2012) 83–89.
[65] J.R. Li, R.J. Kuppler, H.C. Zhou, Selective gas adsorption and separation in metal-organic frameworks, Chem. Soc. Rev. 38 (2009) 1477–1504.
[66] M.D. Allendorf, C.A. Bauer, R.K. Bhakta, R.J.T. Houk, Luminescent metal-organic frameworks, Chem. Soc. Rev. 38 (2009) 1330–1352.
[67] S.S. Han, S.-H. Choi, W.A. Goddard, III., Improved H2 storage in zeolitic imidazolate frameworks using Li+, Na+, and K+ dopants, with an emphasis of delivery H2 uptake, J. Phys. Chem. C 115 (2011) 3507–3512.
[68] N.S. Bobbitt, J. Chen, R.Q. Snurr, High-throughput screening of metal-organic frameworks for hydrogen storage at cryogenic temperature, J. Phys. Chem. C 120 (2016) 27328–27341.
[69] J. Fu, Y. Liu, Y. Tian, J. Wu, Density functional methods for fast screening of metal-organic frameworks for hydrogen storage, J. Phys. Chem. C 119 (2015) 5374–5385.
[70] D. Gygi, E.D. Bloch, J.A. Mason, M.R. Hudson, M.I. Gonzalez, R.L. Siegelman, T. A. Darwish, W.L. Queen, C.M. Brown, J.R. Long, Hydrogen storage in the expanded pore metal-organic frameworks M2(dobpdc) (M = Mg, Mn, Fe, Co, Ni, Zn), Chem. Mater. 28 (2016) 1128–1138.
[71] R. Vaidhyanathan, D. Bradshaw, J.N. Rebilly, J.P. Barrio, J.A. Gould, N.G. Berry, M.J. Rosseinsky, A family of nanoporous materials based on an amino acid backbone, Angew. Chem. 118 (2006) 6645–6649.
[72] C. Wu, W. Lin, Heterogeneous asymmetric catalysis with homochiral metal-organic frameworks: network-structure-dependent catalytic activity, Angew. Chem. 119 (2007) 1093–1096.
[73] S.H. Cho, B.Q. Ma, S.T. Nguyen, J.T. Hupp, T.E. Albrecht- Schmitt, A metal-organic framework material that functions as an enantioselective catalyst for olefin epoxidation, Chem. Commun. 2563−2565 (2006).
[74] S.S. Han, D.H. Jung, J. Heo, Interpenetration of metal organic frameworks for carbon dioxide capture and hydrogen purification: good or bad? J. Phys. Chem. C 117 (2013) 71–77.
[75] S. Li, Y.G. Chung, R.Q. Snurr, High-throughput screening of metal-organic frameworks for CO_2 capture in the presence of water, Langmuir 32 (2016) 10368–10376.
[76] H. Demir, C.J. Cramer, J.I. Siepmann, Computational screening of metal-organic frameworks for biogas purification, Mol. Syst. Des. Eng. 4 (2019) 1125–1135.
[77] H. Huang, W. Zhang, D. Liu, C. Zhong, Understanding the effect of trace amount of water on CO_2 capture in natural gas upgrading in metal-organic frameworks: a molecular simulation study, Ind. Eng. Chem. Res. 51 (2012) 10031–10038.
[78] J. Park, H. Kim, S.S. Han, Y. Jung, Tuning metal-organic frameworks with open metal sites and its origin for enhancing CO_2 affinity by metal substitution, J. Phys. Chem. Lett. 3 (2012) 826–829.
[79] N.C. Burtch, H. Jasuja, K.S. Walton, Water stability and adsorption in metal–organic frameworks, Chem. Rev. 114 (20) (2014) 10575–10612.
[80] Y. Li, Z. Ju, B. Wu, D. Yuan, A water and thermally stable metal–organic framework featuring selective CO2 adsorption, Cryst. Growth Des. 13 (9) (2013) 4125–4130.
[81] K. Tan, N. Nijem, P. Canepa, Q. Gong, J. Li, T. Thonhauser, Y.J. Chabal, Stability and hydrolyzation of metal organic frameworks with paddle-wheel SBUs upon hydration, Chem. Mater. 24 (16) (2012) 3153–3167.
[82] S. Han, Y. Huang, T. Watanabe, S. Nair, K.S. Walton, D.S. Sholl, J.C. Meredith, MOF stability and gas adsorption as a function of exposure to water, humid air, SO2, and NO2, Microporous Mesoporous Mater. 173 (2013) 86–91.
[83] S. Zuluaga, E.M. Fuentes-Fernandez, K. Tan, F. Xu, J. Li, Y.J. Chabal, T. Thonhauser, Understanding and controlling water stability of MOF-74, J. Mater. Chem. A 4 (14) (2016) 5176–5183.
[84] X.Y. Chen, H. Vinh-Thang, A.A. Ramirez, D. Rodrigue, S. Kaliaguine, Membrane gas separation technologies for biogas upgrading, RSC Adv. 5 (31) (2015) 24399–24448.
[85] E.V. Perez, K.J. Balkus Jr., J.P. Ferraris, I.H. Musselman, Mixed-matrix membranes containing MOF-5 for gas separations, J. Membr. Sci. 328 (1–2) (2009) 165–173.
[86] A.W. Thornton, R. Babarao, A. Jain, F. Trousselet, F.X. Coudert, Dalton Trans. 45 (2016) 4352–4359.
[87] L. Sarkisov, Molecular simulation of low temperature argon adsorption in several models of IRMOF-1 with defects and structural disorder, Dalton Trans. 45 (2016) 4203–4212.
[88] Y. Basdogan, S. Keskin, Simulation and modelling of MOFs for hydrogen storage, CrystEngComm 17 (2015) 261–275.
[89] S. Vellamarthodika, S. Gautam, Role of orientational disorder in ZSM-22 in the adsorption of SO_2, Mol. Phys. 120 (2022) e2117663.
[90] I. Dhiman, M.C. Berg, David R. Cole, S. Gautam, Correlation between structure and dynamics of CO_2 confined in mg-MOF-74 and the role of inter-crystalline space: a molecular dynamics simulation study, Appl. Surf. Sci. 612 (2023) 155909.
[91] A.O. Yazaydin, R.Q. Snurr, T.H. Park, K. Koh, J. Liu, M.D. LeVan, A.I. Benin, P. Jakubczak, M. Lanuza, D.B. Galloway, J.J. Low, R.R. Willis, Screening of metal-organic frameworks for carbon dioxide capture from flue gas using a combined experimental and modeling approach, J. Am. Chem. Soc. 131 (2009) 18198–18199.
[92] https://github.com/numat/RASPA2/blob/master/structures/mofs/cif/MgMOF-74.cif.
[93] I. Dhiman, S. Vellamarthodika, S. Gautam, Influence of orientational disorder in the adsorbent on the structure and dynamics of the adsorbate: MD simulations of SO2 in ZSM-22, Chem. Eng. Sci. 283 (2024) 119389.
[94] J.A. Purton, J.C. Crabtree, S.C. Parker, Mol. Simul. 39 (2013) 1240–1252.
[95] S. Bendt, Y. Dong, F.J. Keil, Diffusion of water and carbon dioxide and mixtures thereof in mg-MOF-74, J. Phys. Chem. C 123 (13) (2019) 8212–8220.
[96] J.J. Potoff, J.I. Siepmann, Vapor–liquid equilibria of mixtures containing alkanes, carbon dioxide, and nitrogen, AICHE J. 47 (2001) 1676–1682.
[97] M.G. Martin, J.I. Siepmann, Transferable potentials for phase equilibria. 1. United-atom description of n-alkanes, J. Phys. Chem. B 102 (1998) 2569–2577.
[98] P.D.C. Dietzel, V. Besikiotisa, R. Bloma, Application of metal–organic frameworks with coordinatively unsaturated metal sites in storage and separation of methane and carbon dioxide, J. Mater. Chem. 19 (2009) 7362–7370.
[99] R. Krishna, J.M. van Baten, Investigating the potential of mg-MOF-74 membranes for CO_2 capture, J. Membr. Sci. 377 (2011) 249–260.
[100] I.T. Todorov, W. Smith, K. Trachenko, M.T. Dove, DL_POLY_3: new dimensions in molecular dynamics simulations via massive parallelism, J. Mater. Chem. 16 (2006) 1911–1918.
[101] S. Gautam, D.R. Cole, CO_2 adsorption in metal-organic framework mg-MOF-74: effects of inter-crystalline space, Nanomaterials 10 (2020) 2274.
[102] S. Gautam, D.R. Cole, Effects of inter-crystalline space on the adsorption of ethane and CO_2 in silicalite: implications for enhanced adsorption, Phys. Chem. Chem. Phys. 22 (2020) 13951–13957.
[103] S. Gautam, D.R. Cole, Ethane-CO_2 mixture adsorption in Silicalite: influence of tortuosity and connectivity of pores on selectivity, J. Car. Res. 9 (2023) 116.
[104] Z. Bao, L. Yu, Q. Ren, X. Lu, S. Deng, Adsorption of CO_2 and CH_4 on a magnesium-based metal organic framework, J. Colloid Interface Sci. 353 (2011) 549–556.
[105] G. Zhang, Y. Liang, G. Cui, B. Dou, W. Lu, Q. Yang, X. Yan, Grand canonical Monte Carlo simulation of the adsorption and separation of carbon dioxide and methane using functionalized mg-MOF-74, Energy Rep. 9 (2023) 2852–2860.
[106] T. Le, A. Striolo, D.R. Cole, CO_2-C_4H_{10} mixtures simulated in silica slit pores: relation between structure and dynamics, J. Phys. Chem. C 119 (2015) 15274–15284.
[107] S. Gautam, T. Liu, G. Rother, N. Jalarvo, E. Mamontov, S. Welch, J. Sheets, M. Droege, D.R. Cole, Dynamics of propane in Nanoporous silica aerogel: a Quasielastic neutron scattering study, J. Phys. Chem. C 119 (2015) 18188–18195.
[108] M. Linares-Moreau, L.A. Brandner, M.D.J. Velásquez-Hernández, J. Fonseca, Y. Benseghir, J.M. Chin, D. Maspoch, C. Doonan, P. Falcaro, Fabrication of oriented polycrystalline MOF superstructures, Adv. Mater. 36 (1) (2024) 2309645.